Theoretical Insights into the Aggregation-Induced Emission by Hydrogen Bonding: A QM/MM Study

ARTICLE *in* THE JOURNAL OF PHYSICAL CHEMISTRY A · APRIL 2012

Impact Factor: 2.69 · DOI: 10.1021/jp3002367 · Source: PubMed

5 AUTHORS, INCLUDING:

Qunyan Wu
Tsinghua University
15 PUBLICATIONS **125** CITATIONS
SEE PROFILE

Qian Peng
Chinese Academy of Sciences
66 PUBLICATIONS **1,421** CITATIONS
SEE PROFILE

Xing Gao
Max Planck Institute for Coal Research
7 PUBLICATIONS **145** CITATIONS
SEE PROFILE

Zhigang Shuai
Tsinghua University
319 PUBLICATIONS **10,090** CITATIONS
SEE PROFILE

THE JOURNAL OF PHYSICAL CHEMISTRY A

Article

pubs.acs.org/JPCA

Theoretical Insights into the Aggregation-Induced Emission by Hydrogen Bonding: A QM/MM Study

Qunyan Wu,[†] Qian Peng,[‡] Yingli Niu,[‡] Xing Gao,[†] and Zhigang Shuai*[,†,‡]

[†]MOE Key Laboratory of Organic OptoElectronics and Molecular Engineering, Department of Chemistry, Tsinghua University, Beijing 100084, People's Republic of China

[‡]Key Laboratory of Organic Solids, Beijing National Laboratory for Molecular Science (BNLMS), Institute of Chemistry, Chinese Academy of Sciences, Beijing 100190, People's Republic of China

Supporting Information

ABSTRACT: We investigate the excited-state decay processes for the 3-(2-cyano-2- phenylethenyl-Z)-NH-indole (**CPEI**) in the solid phase through combined quantum mechanics and molecular mechanics (QM/MM) and vibration correlation formalisms for radiative and nonradiative decay rates, coupled with time-dependent density functional theory (TDDFT). By comparing the isolated **CPEI** molecule and the molecule-in-cluster, we show that the molecular packing through intermolecular hydrogen-bonding interactions can hinder the excited-state nonradiative decay and thus enhance the fluorescence efficiency in the solid phase. Aggregation effect is shown to block the nonradiative decay process through hindering the low-frequency vibration motions. The fluorescence quantum yields for both isolated molecule and aggregation are predicted to be insensitive to temperature due to the hydrogen-bonding nature, and their values at room temperature are consistent with the experiment.

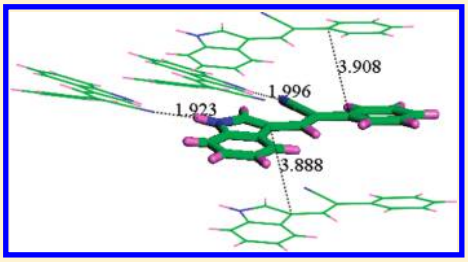

I. INTRODUCTION

Molecules with aggregation-induced emission (AIE) phenomena have attracted a lot of attention in recent years.[1,2] A series of luminogens have been found to demonstrate aggregation enhanced light emitting; their aggregates and/or solid phases manifest much stronger light emission than in dilute solutions, in sharp contrast to the traditional aggregation quenching.[1−9] Optoelectronic devices, such as organic light-emitting diodes (OLEDs),[10] operate in the solid state. However, highly efficient emission from organic materials is often prohibited by the concentration quenching of the luminescence in the solid state, due to electron transfer, or energy transfer, or Davydov splitting, which could be a thorny obstacle to the application of efficient light-emitting devices.[11]

Great progress has been achieved in understanding ultrafast processes for complex molecules in dilute solutions.[12] It is still challenging to investigate these processes in aggregate or solid state. It is intriguing to understand the mechanism of AIE phenomena. Several explanations of AIE have been proposed, which need to be clarified, including the restriction of intramolecular rotations,[5] J-aggregate formation,[6] excimer emission,[7] intramolecular planarization and intermolecular interactions,[8] or intramolecular charge transfer.[9] Furthermore, hydrogen-bonding assisted enhancement of fluorescence emissions has also been reported by several groups.[8,13,14] Theoretically, Yin et al. have first carried out quantum chemical calculations for the excited-state vibronic coupling for silole derivatives.[15] It was found that the low-frequency phenyl ring twisting motions tend to strongly dissipate the electronic excited-state energy. In addition, it was shown that isopropyl substitution at proper sites can cause severe hindrance to the phenyl ring twisting, which eventually blocks the nonradiative decay channel as evidenced from the first-principles calculation of nonradiative decay rates. Peng et al. further pointed out that the molecular vibration modes with low-frequency tend to mix each other upon photoexcitation, and such mixing known as the Duschinsky rotation effect (DRE) can strongly enhance the nonradiative energy dissipation process due to the outspreads of Franck−Condon factors among different normal modes at increasing temperature.[16] The AIE phenomenon was understood from the calculations of nonradiative decay processes as a function of temperature in tetraphenylbutadienes: lowering the temperature resembles to some extent the aggregate effect. Upon increasing temperature, the vibration quanta are becoming larger, and the low-frequency modes are getting coupled to each other through DRE, which greatly increases the nonradiative decay rate.[16] The most recent calculations on the radiative and nonradiative decay processes in pyrazine derivatives also confirmed such trends; for compound with floppy phenyl rings, the temperature dependence of radiationless decay is much more pronounced than in the rigid compound.[17]

These previous theoretical studies have focused on isolated molecule; the molecular origin of AIE and the temperature effect have been investigated by mimicking aggregate through lowering temperature. It is primarily the purpose of this study

Received: January 8, 2012
Revised: March 28, 2012
Published: March 28, 2012

to look at the photophysical properties in the condensed phase from quantum chemical calculations. Here, we investigated explicitly the molecular aggregation influences on both the radiative and the nonradiative decays of 3-(2-cyano-2-phenylethenyl-Z)-NH-indole (**CPEI**)[13] (Scheme 1) by a quantum

Scheme 1. Structure of 3-(2-Cyano-2-phenylethenyl-Z)-NH-indole Molecule

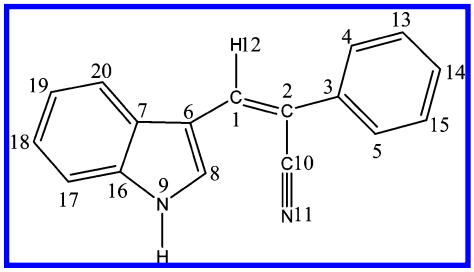

mechanics and molecular mechanics (QM/MM) approach coupled with a more elaborate formalism for treating nonradiative decay of the molecular excited state. Experimentally, **CPEI** is almost nonemissive in tetrahydrofuran (THF) solution with a tiny fluorescence quantum yield (<0.001).[13] However, when mixing 90% volume fraction of water in THF, **CPEI** becomes strongly emissive. In fact, the polarity of water is very different from THF. So, when increasing the water fraction, **CPEI** molecules start to aggregate, to form small clusters in solution. The fluorescence emission intensity at 99% water fraction is about 18 times as much as that at 20%. The solid-state fluorescence quantum yield was measured to be 0.192, and such a huge enhancement (from <0.001) was ascribed to the intramolecular planarization and restricted twisted motions of the molecule.[13] In this work, we apply the quantum chemical method to quantitatively calculate the radiative and nonradiative decay rates for **CPEI** at both gas phase and for molecule-in-cluster to gain deeper insights into the AIE phenomena.

II. METHODOLOGICAL APPROACHES

The molecular light-emitting efficiency is determined by the competition between the radiative decay rate (k_r) and the nonradiative decay rate (k_{nr}). The fluorescence quantum yield can be expressed as $\eta_f = k_r/(k_r + k_{nr})$. Therefore, either suppressing the nonradiative rate or increasing the radiative rate can attain higher fluorescence efficiency. k_{nr} is generally a sum of the internal conversion rate (k_{ic}) and the intersystem crossing rate (k_{isc}).

Simulating excited-state dynamics is a formidable challenge for theoretical chemistry. There has been progress in photoinduced electron dynamics,[18] for example, by the Ehrenfest dynamics,[19] surface hopping dynamics,[20] or the multiconfigurational time-dependent Hartree (MCTDH) algorithm,[21] which has been successfully applied to study the nonadiabatic electron dynamics for molecular photodissociation and photoexcitation phenomena.[22] However, these approaches describe typically a subpicosecond process ($<10^{-12}$ s), in general, until the conical intersection occurs. Simulation for longer time poses difficulties either in computational costs or in error control. Such time scale is much shorter than the typical excited-state process in organic light-emitting materials, $\sim 10^{-7}$–10^{-8} s.[23] Furthermore, the light-emitting device works in the solid state; therefore, the photochemical reaction or conical intersection should not be the dominant process. Otherwise, the device would degrade immediately, which is not the case. For complex polyatomic molecule, the degrees of freedom of nuclear motions are usually large, and each of them could be reasonably assumed to move not far away from the equilibrium upon photo- or electro-excitation. In fact, a recent work by Jiang et al. showed that as the chain length of oligo-thienylenevinylene increases, the vibration quanta for IC process decreases steadily.[24] For a large degree of freedom, the harmonic oscillator model could be a suitable choice. So, in this work, we employ a statistical rate formalism to describe the excited-state decay processes.

The radiative decay rate can be computed by the Einstein spontaneous emission rate, which eventually can be expressed by the integration over the whole emission spectrum:

$$k_r(T) = \int \sigma_{em}(\omega, T)\mathrm{d}\omega \tag{1}$$

where

$$\sigma_{em}(\omega, T) = \frac{4\omega^3}{3\hbar c^3} \sum_{\nu_i \nu_f} P_{i\nu_i}(T) |\langle \Theta_{f\nu_f} | \vec{\mu}_{fi} | \Theta_{i\nu i} \rangle|^2 \delta(\omega_{i\nu_i f\nu_f} - \omega) \tag{2}$$

$\vec{\mu}_{fi} = \langle \Phi_f | \vec{\mu} | \Phi_i \rangle$ is the electric transition dipole moment between two electronic states $|\Phi_i\rangle$ and $|\Phi_f\rangle$, and can be expanded in the normal coordinates as:

$$\vec{\mu}_{fi} = \vec{\mu}_0 + \sum_k \vec{\mu}_k Q_k + \sum_{k,l} \vec{\mu}_{kl} Q_k Q_l + \ldots \tag{3}$$

Considering the strongly dipole-allowed transitions of the molecules in this work, only the zeroth-order term $\vec{\mu}_0$ (Franck–Condon approximation, FC) is taken into account. $P_{i\nu_i}$ is the Boltzmann distribution function for the initial state vibronic manifold. Φ and Θ are the electronic and vibrational wave functions, respectively. Applying the Fourier transformation to the delta function in eq 2, we can obtain an analytical integral formalism:

$$\sigma_{em}^{FC}(\omega) = \frac{2\omega^3}{3\pi\hbar c^3} |\vec{\mu}_0|^2 \int_{-\infty}^{\infty} e^{-i(\omega - \omega_{if})t} Z_{i\nu}^{-1} \rho_{em,0}^{FC}(t, T)\mathrm{d}t \tag{4}$$

Here, $Z_{i\nu}$ is the partition function, and $\rho_{em,0}^{FC}(t, T) = \mathrm{Tr}[e^{-i\tau_f \hat{H}_f} e^{-i\tau_i \hat{H}_i}]$ is the correlation function, where $\tau_i = -i\beta - t/\hbar$, $\tau_f = t/\hbar$, and $\beta = (k_B T)^{-1}$, k_B is the Boltzmann constant. $\hat{H}_f$ and $\hat{H}_i$ are the multidimensional harmonic oscillator Hamiltonians for the final and initial electronic states, respectively. The correlation function in eq 4 had been solved analytically by virtue of multidimensional Gaussian integrations in the path integral framework:[25]

$$\rho_{em,0}^{FC}(t, T) = \sqrt{\frac{\det[a_f a_i]}{\det[K]}} \exp\left\{ -\frac{i}{\hbar} \left[\frac{1}{2} \underline{F}^T K \underline{F} - \underline{D}^T E \underline{D} \right] \right\} \tag{5}$$

where a_i, a_f, and E are $(N \times N)$ matrices, K is $(2N \times 2N)$ matrix, and $\underline{D}$ and $\underline{F}$ are $(N \times 1)$ and $(2N \times 1)$ matrices, respectively, with all of the mathematical forms given in our previous work.[26]

The nonradiative internal conversion (IC) processes had been investigated theoretically by Huang and Rhys in solid-state physics[27] and by Lin et al.[28] for molecules within the

dx.doi.org/10.1021/jp3002367 | J. Phys. Chem. A 2012, 116, 3881–3888

displaced harmonic oscillator model. According to Fermi's golden rule, the IC rate can be expressed as

$$k_{ic} = \frac{2\pi}{\hbar}|H'_{fi}|^2\delta(E_{fi} + E_{fv_f} - E_{iv_i}) \quad (6)$$

Here, the perturbation H' is the non-Born−Oppenheimer coupling:

$$H'_{fi} = -\hbar^2 \sum_l \left\langle \Phi_f\Theta_{fv_f}|\frac{\partial\Phi_i}{\partial Q_{fl}}\frac{\partial\Theta_{iv_i}}{\partial Q_{fl}}\right\rangle \quad (7)$$

Applying the Condon approximation, eq 7 becomes

$$H'_{fi} = \sum_l \langle\Phi_f|\hat{P}_{fl}|\Phi_i\rangle\langle\Theta_{fv_f}|\hat{P}_{fl}|\Theta_{iv_i}\rangle \quad (8)$$

Here, $\hat{P}_{fl} = -i\hbar(\partial/(\partial Q_{fl}))$ is the normal momentum operator. Inserting eq 8 into eq 6, the IC rate can be expressed as

$$k_{IC} = \sum_{kl} k_{ic,kl} \quad (9)$$

with

$$k_{ic,kl} = \frac{2\pi}{\hbar}R_{kl}Z_{iv}^{-1}\sum_{v_i,v_f} e^{-\beta E_{iv_i}}P_{kl}\delta(E_{fi} + E_{fv_f} - E_{iv_i}) \quad (10)$$

and

$$R_{kl} = \langle\Phi_f|\hat{P}_{fk}|\Phi_i\rangle\langle\Phi_i|\hat{P}_{fl}|\Phi_f\rangle \quad (11)$$

$$P_{kl} = \langle\Theta_{fv_f}|\hat{P}_{fk}|\Theta_{iv_i}\rangle\langle\Theta_{iv_i}|\hat{P}_{fl}|\Theta_{fv_f}\rangle \quad (12)$$

The electronic nonadiabatic coupling term arising from the lth normal mode can be defined as $V_l = ((1/2)\hbar\omega_l R_{ll})^{1/2}$, which contains only the diagonal contribution and has a dimension of energy, in parallel to the charge transfer rate formula.

The delta function in eq 10 is Fourier transformed as

$$k_{ic,kl} = \frac{1}{\hbar^2}R_{kl}\int_{-\infty}^{\infty} dt[e^{i\omega_{if}t}Z_{iv}^{-1}\rho_{ic,kl}(t, T)] \quad (13)$$

where $\rho_{ic,kl}(t,T)$ is the thermal vibrational correlation function in the internal conversion process:

$$\rho_{ic,kl}(t, T) = Tr(\hat{P}_{fk}e^{-i\tau_f\hat{H}_f}\hat{P}_{fl}e^{-i\tau_i\hat{H}_i}) \quad (14)$$

We have derived an analytical expression for eq 14:[26,27,29]

$$\rho_{ic,kl}(t, T) = \sqrt{\frac{\det[a_f a_i]}{\det[K]}}\exp\left\{-\frac{i}{\hbar}\left[\frac{1}{2}\underline{F}^T K^{-1}\underline{F} - \underline{D}^T E\underline{D}\right]\right\} \times \{i\hbar Tr[G_{kl}K^{-1}] + (K^{-1}\underline{F})^T G_{kl}(K^{-1}\underline{F}) - (H_{kl})^T K^{-1}\underline{F}\} \quad (15)$$

Here, a_i, a_f, and E are $(N \times N)$ matrices, K is $(2N \times 2N)$ matrix, $\underline{D}$ is $(N \times 1)$ matrix, $\underline{F}$ is $(2N \times 1)$ matrix, and G_{kl} and H_{kl} are the $(2N \times 2N)$ and $(1 \times 2N)$ matrices, respectively, with all of the mathematical forms given in our previous work.[26] The advantages of such correlation function formalism lie in that (i) it is fully analytical; (ii) the vibration modes mixing effect has been fully taken into account,[29] which was shown to be essential for low frequency motions because these modes become mixed when the electronic state is excited, expressed as $Q_k^e = \sum_j S_{kj}Q_j^g + D_k$, where S_{kj} is the Duschinsky rotation matrix elements and the vector D_k is the rigid shift in potential energy surface minimum, often quantified by Huang−Rhys factor $HR_k = \omega_k D_k^2/2\hbar$;[15,29,30] and (iii) all of the vibration modes are taken into account when evaluating the nonadiabatic transition moment R_{kl}, including both diagonal and nondiagonal, instead of selecting only one specific mode called the "promoting mode" in previous theory.[28]

Such formalism has been shown to be reasonable in describing the photophysical properties for organic polyatomic systems when conical intersection (CI) is not involved: the decay rate of CI is usually greater than 10^{12} s^{-1}. Our formalism is only applicable for excited-state decay rate less than 10^{12} s^{-1}. Otherwise, the rate assumption should be cautioned. All of the molecular parameters required in this formalism can be computed by DFT/TDDFT, including the vertical and adiabatic molecular excited-state energies, the harmonic vibrational frequencies for the QM region including the MM environment, and the displacement vectors D_k between the excited-state and the ground-state parabola. Duschinsky rotation matrix and the displacement vector are calculated as outlined in ref 26 by following Reimers.[31]

III. COMPUTATIONAL DETAILS

The geometry optimization and harmonic vibrational frequency calculations of the isolated **CPEI** molecule were carried out with the Turbomole 6.3 program package.[32] The ground-state geometry optimization was started with an initial guess from the X-ray diffraction crystal structure[13] at the level of density functional theory (DFT). For the first singlet excited electronic state, TDDFT was applied. The EGRAD module, which provides TDDFT analytic energy gradients for optimization, was employed.[33] The energy convergence thresholds for the ground state ($\mathbf{S_0}$) and the first singlet excited electronic state ($\mathbf{S_1}$) optimization were set to be 10^{-9} atomic unit. It should be noted that TDDFT with common exchange correlation functional works well only for the low-lying excited state with mostly single excitation character.[33] We will see that the first singlet excited state of **CPEI** molecule consists of primarily HOMO − LUMO promotion. Therefore, it is appropriate to apply TDDFT.

QM/MM has been extensively used for dealing with numerous complex systems in chemical phenomena.[34] It partitions the system into a QM region with chemical interests and an MM region for the surrounding chemical environments. Here, we model the aggregation effect on a single molecule (QM) through taking electrostatic interaction with neighboring molecules (MM), and the charge transfer between QM and MM regions is ignored. Our setup of computational model is shown in Figure 1, where a cluster of 75 **CPEI** molecules is cut from the X-ray diffraction crystal structure,[13] consisting of 31 QM atoms and 2294 MM atoms. The QM/MM calculations were performed with the ChemShell 3.4 interface package,[35] where the geometry optimization is done through the HDLC (hybrid delocalized internal coordinate) optimizer.[36] Turbomole 6.3 and the DL-POLY program package[37] were used to calculate the energies and gradients of the QM and MM region, respectively. All QM calculations were carried out using B3LYP/SV(P), and the TDDFT method was applied to optimize the first singlet excited electronic state geometries. The MM part is treated with the General Amber Force Field (GAFF).[38] The electrostatic embedding scheme was applied in the QM/MM calculations;[39] the MM charges were incorporated into the one-electron part of the QM Hamiltonian, and the QM/MM electrostatic interactions were evaluated from the QM electrostatic potential and the MM partial charges. The intermolecular electrostatic interaction can influence the $\mathbf{S_0}$ and

dx.doi.org/10.1021/jp3002367 | J. Phys. Chem. A 2012, 116, 3881−3888

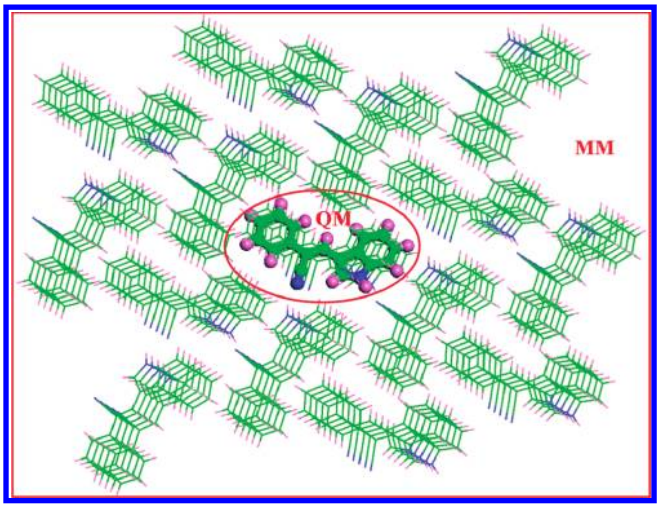

Figure 1. Setup of our QM/MM model for a cluster with 75 **CPEI** molecules cut from the crystal structure with the central one as QM region.

S_1 structures as well as their vibronic couplings for the QM region. We have tested two schemes for choosing active region for geometry optimization: one with only QM molecule and another with 15 molecules (one QM molecule plus surrounding 14 MM molecules). The difference in bond lengths obtained is less than 0.01 Å. Thus, in the following computations, only the QM molecule is chosen as the active region for optimization. In this work, we did not consider intermolecular charge transfer excitation and the excitonic effect, which are beyond the reach of the present methodology. In fact, for most of the molecular crystal, the lowest optical excitation is of Frenkel intramolecular excitation type, and the AIE phenomena have been studied in general for amorphously aggregated clusters of molecules, while the exciton effect is only pronounced in well-ordered crystals. Nevertheless, we believe both charge transfer and excitonic effects pose important challenges in studying the AIE phenomena, which deserve further investigation in the future.

Harmonic vibrational frequencies were calculated at the equilibrium geometries of the S_0 and S_1. The atomic electric field transition moment required by the electronic nonadiabatic coupling term V_l for the internal conversion rate is calculated at the TDDFT level by using the Gaussian 09 program.[40] On the basis of the electronic structure information of the QM part, the Duschinsky rotation matrix and the normal mode displacements between the two electronic states, as well as the radiative and nonradiative decay rates, were calculated.

IV. RESULTS AND DISCUSSION

A. Geometry and Normal Modes Analysis. The selected bond lengths, bond angles, and dihedral angles of the S_0 and S_1 for the isolated **CPEI** molecule with QM method and the molecule-in-cluster with QM/MM approach are shown in Table 1. The total energy as well as the vertical and adiabatic transition energies both for isolated molecule and for molecule-in-cluster are given in Table 2. A close look at the intermolecular hydrogen bonding is shown in Figure 2.

Table 2. Total Energy of the Ground State $[E(S_0)]$ and the First Excited State $[E(S_1)]$, Adiabatic Excitation Energy ΔE, Vertical Transition Energy from S_0 to S_1 ($E_{v(gs)}$), and Vertical Transition Energy from S_1 to S_0 ($E_{v(es)}$), Both for Isolated Molecule and for Molecule-in-Cluster

	$E(S_0)$ [au]	$E(S_1)$ [au]	ΔE [eV]	$E_{v(gs)}$ [eV]	$E_{v(es)}$ [eV]
isolated molecule	−763.477138	−763.501308	3.26	3.47	2.89
cluster	−763.357495	−763.383119	3.22	3.37	3.03

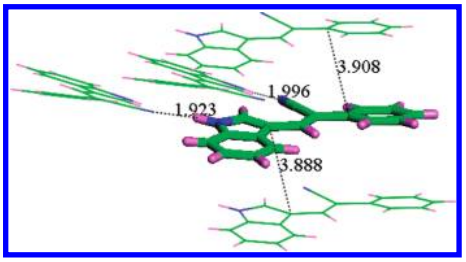

Figure 2. Close look at the molecular packing structure.

From the comparison of geometries for the ground electronic state in the gas phase and in the solid state, it is

Table 1. Selected Bond Lengths (in Å), Angles, and Torsion Angles (in deg) of the S_0 and S_1 for Isolated CPEI Molecule and Molecule-in-Cluster

	isolated molecule			molecule-in-cluster			
	S_0	S_1	$\Delta(S_0-S_1)$	S_0	S_1	$\Delta(S_0-S_1)$	expr.[a]
C_1-C_2	1.371	1.440	−0.069	1.373	1.429	−0.056	
C_2-C_3	1.488	1.447	0.041	1.486	1.451	0.036	
C_1-C_6	1.442	1.414	0.029	1.437	1.424	0.014	
C_2-C_{10}	1.433	1.419	0.015	1.431	1.419	0.013	
N_9-H	1.013	1.014	−0.001	1.022	1.023	−0.001	
$C_1-C_2-C_3$	123.77	121.98	1.79	124.25	121.74	2.51	
$C_2-C_3-C_4$	121.82	121.46	0.36	122.10	121.64	0.46	
$C_2-C_1-C_6$	130.81	126.01	4.80	131.37	127.09	4.28	
$C_1-C_6-C_7$	124.13	126.19	−2.06	123.91	124.86	−0.95	
$C_1-C_6-C_8$	130.17	128.71	1.46	130.60	130.34	0.26	
$C_6-C_1-C_2-C_3$	179.17	159.38	19.79	178.00	177.10	0.90	
$C_1-C_2-C_3-C_4$	−21.77	−6.57	−15.20	−12.29	−9.20	−3.09	9.0
$C_2-C_1-C_6-C_8$	−2.42	−4.25	1.83	−0.49	−1.42	0.93	−1.2

[a]Reference 13.

dx.doi.org/10.1021/jp3002367 | J. Phys. Chem. A 2012, 116, 3881−3888

seen that the bond lengths are almost the same except for the N_9−H bond, which in the gas phase is 1.013 Å, while in the solid state it is 1.022 Å, due to the formation of an intermolecular hydrogen bond between N_9−H of the indolic ring and the N_{11} atom of the $C_{10}N_{11}$ group in the neighboring molecule; see Figure 2. The lengths of the two N_9−H···N_{11} hydrogen bonds are 1.923 and 1.996 Å, respectively. The dihedral angles C_1−C_2−C_3−C_4 and C_2−C_1−C_6−C_8 are −21.77° and −2.42° for the S_0 in the isolated **CPEI** molecule, while the corresponding values become −12.29° and −0.49° in the solid state, which demonstrated that the intermolecular hydrogen-bond interactions greatly increase the rigidity of the molecule by restricting the intramolecular rotation. Moreover, the two predicted dihedral angles in the solid state with QM/MM approach are in good agreement with X-ray diffraction analysis (9.0° and 1.2°),[13] which indicated the reliability of our QM/MM approach for determining the geometry. As shown in Table 1, the modifications of the two dihedral angles C_1−C_2−C_3−C_4 and C_2−C_1−C_6−C_8 from the S_1 to S_0 are 15.20° and 1.83° for the isolated **CPEI** molecule, while these become 3.09° and 0.93° in the solid state. This showed that when the electronic state changes from S_1 to S_0, the molecular structure becomes much more rigid in the solid state than in the gas phase; that is, the rotations of the rings for the excited state are hindered in the cluster due to the molecular packing and the intermolecular hydrogen-bonding interactions. It should be pointed out that the main conjugation backbone (C_1=C_2) of the **CPEI** molecule is much more planar in the solid state for both the excited and ground states, with the dihedral angle C_6−C_1−C_2−C_3 slightly changing from 178.00° to 177.10°, while in the isolated **CPEI** molecule, the dihedral angle undergoes more pronounced modification, from 179.17° to 159.38°. We plot the potential energy curves along the C_6−C_1−C_2−C_3 torsion angle of the ground state for the isolated **CPEI** molecule in comparison with molecule-in-cluster in Figure 3. It is clearly

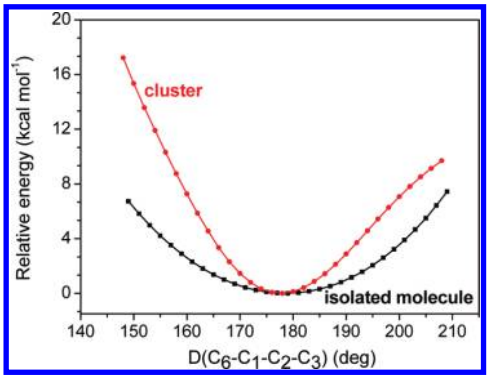

Figure 3. Potential energy curves along the torsion angle (C_6−C_1−C_2−C_3) of the ground state for the isolated **CPEI** molecule (black line) and the cluster (red line).

seen that the torsional motion for the dihedral angle C_6−C_1−C_2−C_3 for molecule-in-cluster costs higher energy than that in the isolated molecule.

TDDFT calculations show that S_1 is dominated by the transition from the HOMO to the LUMO for both the isolated **CPEI** molecule (98.2%) and the molecule-in-cluster (97.9%). The HOMO and LUMO display the π and π^* character as shown in Figure 4, which justify our approximation of neglecting the intersystem crossing process.

The normal modes analysis for S_0 and S_1 in the gas phase and in the solid state is reported in Tables S1−S4. The lowest four modes in the isolated **CPEI** molecule belong to the rotations of the indole and phenyl ring, as shown in Figure S1. Their frequencies are 27, 41, 58, and 68 cm^{-1}, much lower than those (105, 119, 143, and 156 cm^{-1}) of the molecule-in-cluster. This again demonstrated the intramolecular rotations are restricted in the cluster. The N−H stretching mode is calculated to be 3604 cm^{-1} (see Table S3) for the isolated **CPEI** molecule, which is remarkably higher than that in the solid state (3527 cm^{-1}, see Table S1). This is a strong evidence of the intermolecular hydrogen-bonding interaction in the aggregate.

B. Photophysical Properties. The electronic nonadiabatic coupling term V_l for all of the normal modes are calculated, and we display some of them with relatively large couplings in Table 3. These contribute to the internal conversion rate, much as the spin−orbital coupling element for the intersystem crossing process. It is seen from Table 3 that the largest V_l value is 65 cm^{-1}. We perform a Complete Active Space Self-Consistent Field (CASSCF) calculation as implemented in MOLPRO package[39] with active space (10, 10) and VDZ basis set for **CPEI**, and we found the spin−orbital coupling constant between S_1 and T_1 is only about 0.1 cm^{-1}. Therefore, we did not consider the intersystem crossing process here.

The calculated radiative decay rate (k_r) and nonradiative decay rate (k_{nr}) with DRE for the isolated molecule and molecule-in-cluster are presented in Table 4. We found that: (i) in all of the cases, the k_r and k_{nr} are insensitive to the temperature; (ii) aggregate strongly influences the nonradiative decay, for example, the k_{nr} for the isolated CPEI molecule at 300 K (3.28×10^{11} s^{-1}) is about 3 orders of magnitude larger than that for the cluster (5.64×10^{8} s^{-1}); therefore from the gas phase to the solid state, the nonradiative decay process has been vastly slowed; and (iii) the molecular aggregate has much less effect on the radiative decay rate k_r, for instance, the k_r is 0.61×10^{8} and 2.17×10^{8} s^{-1} for the isolated molecule and cluster at 300 K, respectively. So far, we did not consider the excitonic effects.[42] In fact, in many of the AIE systems, both the absorption and the emission spectra do not shift appreciably from solution to solid state; that is, the excitonic effect might be prominent for well-ordered single crystal, but might not be the dominant effect for the thin film. Nevertheless, both intermolecular charge transfer and excitonic effects on AIE are not known yet, which caution further theoretical investigations.

The calculated fluorescence quantum yield (η) of the isolated **CPEI** molecule is 1.86×10^{-4} at 300 K, which is in excellent agreement with the experiment (η < 0.001) in THF.[13] The predicted η for the cluster is 0.278, which is also consistent with experimental fluorescence quantum yield (0.192) in the solid state.[13] The fluorescence quantum efficiency is enhanced 1.49×10^{3} times at 300 K due to the aggregation effect. From Table 4, such enhancement is ascribed to the decrease in nonradiative decay rate due to the intermolecular hydrogen-bond interactions and restricted intramolecular rotation at the aggregated state. It is also noted that the temperature dependence of fluorescence quantum yield for aggregate is much less sensitive than that for isolated molecule, indicating the hydrogen-bonding nature, because its strength (4−15 kcal/mol) is much higher than k_BT(300 K) ≈ 0.58 kcal/mol.

C. Huang−Rhys (HR) Factor and Reorganization Energy. Huang−Rhys (HR) factor $HR_j = (\omega_j D_j^2)/2\hbar$

dx.doi.org/10.1021/jp3002367 | J. Phys. Chem. A 2012, 116, 3881−3888

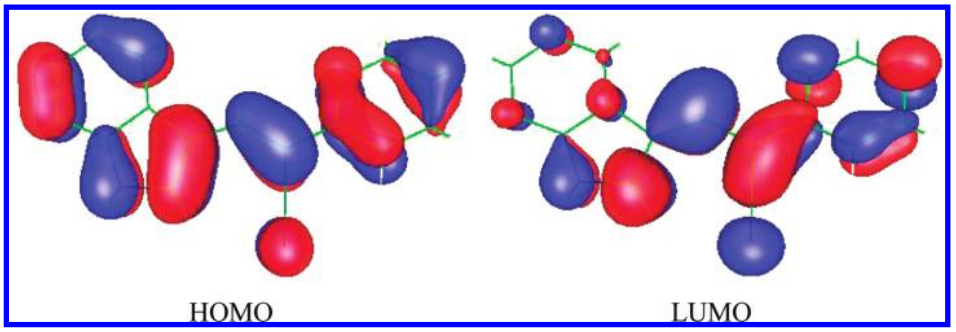

Figure 4. HOMO and LUMO obtained for **CPEI** molecule at the B3LYP/SV(P) level of theory.

Table 3. Selected Nonadiabatic Electronic Coupling Term V_l (in cm^{-1})

mode	V_l	mode	V_l
7	8.094	62	33.326
10	5.104	63	30.928
12	5.584	64	20.902
17	7.005	65	9.924
22	14.903	66	19.617
28	13.045	67	10.607
30	24.960	68	21.189
31	16.890	69	65.431
32	5.182	70	41.769
33	7.979	71	16.325
37	10.015	72	24.295
46	6.963	73	14.711
47	13.163	75	25.749
51	8.213	76	9.360
55	20.395	84	7.392
56	16.464	85	10.361
57	7.768	86	5.022
59	18.514	87	14.889
60	27.872		

characterizes the modification of vibrational quanta (emitting or absorbing) when going from one electronic state to another for the *j*th vibrational mode, which are important for determining the internal conversion rate.[15,16] The HR factors for the S_1 of the isolated **CPEI** molecule and molecule-in-cluster are depicted in Figure S2, and some selected HR factors versus corresponding normal modes are presented in the Supporting Information Tables S5 and S6. It can be seen that the HR factors for the isolated **CPEI** molecule are much larger than those of the molecule-in-cluster. The largest HR factor for the isolated **CPEI** molecule is 6.26 for the mode 1, which corresponds to the rotation of rings as shown in Figure S1, while all of the HR factors for the cluster are much smaller ($HR < 0.31$). These results showed the rotation modes of the rings with lower frequencies are hindered in the solid state because of the intermolecular hydrogen-bonding interactions. Therefore, the energy dissipation via nonradiative channel can be blocked by aggregation, and the radiative decay became dominant in the solid state.

To further understand the relationship between the photophysical properties and the molecular structures, we also plotted the reorganization energies of the first singlet excited state versus corresponding normal modes in Figure 5. The reorganization energy (λ_i) is the product of HR factor and the corresponding vibration energy: $\lambda_i = S_i \times \hbar\omega_i$. The total reorganization energy is 1603 cm^{-1} for the first singlet excited state of the isolated **CPEI** molecule, while it is 1270 cm^{-1} for the molecule-in-cluster, which demonstrate the molecule planarization at aggregation state. The contribution of the low frequency (<100 cm^{-1}) modes to the total reorganization energy is about 24% in isolated molecule, while it is only about 2% in the molecule-in-cluster, which also suggested that the mode of the ring rotation with the lower harmonic vibrational frequencies is the main effect for blocking the nonradiative channel at the aggregated state.

These can be further elucidated by projecting the reorganization energies into the internal coordinate relaxation of the molecules, from Figure 6. The detailed internal coordinates with reorganization energy greater than 10 cm^{-1} are listed in Table S7 for isolated **CPEI** molecule and the molecule-in-cluster. It is worth pointing out that the contributions come from the dihedral angle (37%) relating to the rotation motions of the conjugation backbone $C_1{=}C_2$ plane and the bond length (57%) for the isolated molecule,

Table 4. Calculated Radiative Decay Rate (k_r) and Nonradiative Decay Rate (k_{nr}) from S_1 to S_0 and the Corresponding Fluorescence Quantum Yield (η) at Different Temperatures for Isolated CPEI Molecule and Molecule-in-Cluster

	isolated molecule				molecule-in-cluster			
T [K]	k_r [s^{-1}]	k_{nr} [s^{-1}]	η_{theory}	$\eta_{expr.}$[a]	k_r [s^{-1}]	k_{nr} [s^{-1}]	η_{theory}	$\eta_{expr.}$[a]
300	0.61×10^8	3.28×10^{11}	1.86×10^{-4}	<0.001	2.17×10^8	5.64×10^8	0.278	0.192
250	0.71×10^8	3.21×10^{11}	2.21×10^{-4}		2.19×10^8	5.58×10^8	0.282	
200	0.82×10^8	3.12×10^{11}	2.63×10^{-4}		2.21×10^8	5.53×10^8	0.286	
150	0.96×10^8	3.02×10^{11}	3.18×10^{-4}		2.23×10^8	5.49×10^8	0.289	
100	1.14×10^8	2.83×10^{11}	4.03×10^{-4}		2.24×10^8	5.46×10^8	0.291	
77	1.25×10^8	2.66×10^{11}	4.70×10^{-4}		2.24×10^8	5.45×10^8	0.291	
50	1.38×10^8	2.27×10^{11}	6.08×10^{-4}		2.25×10^8	5.44×10^8	0.293	
20	1.55×10^8	1.41×10^{11}	1.10×10^{-3}		2.25×10^8	5.44×10^8	0.293	

[a]Reference 13.

dx.doi.org/10.1021/jp3002367 | J. Phys. Chem. A 2012, 116, 3881−3888

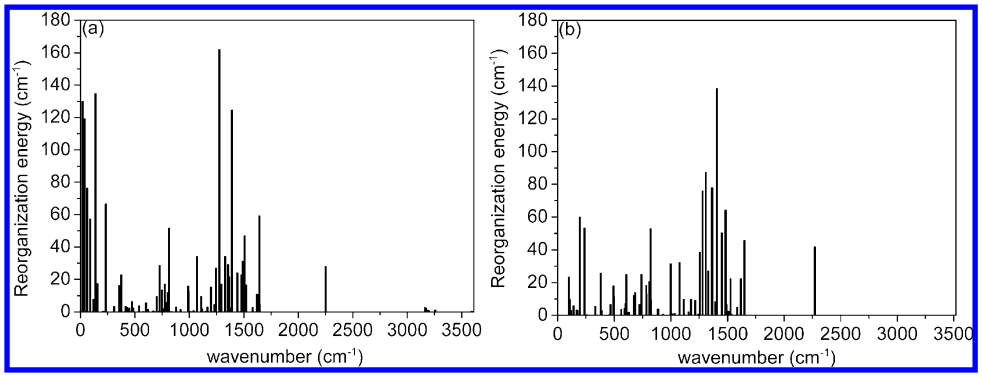

Figure 5. The calculated reorganization energy versus the normal mode wave numbers for (a) isolated **CPEI** molecule and (b) the molecule-in-cluster.

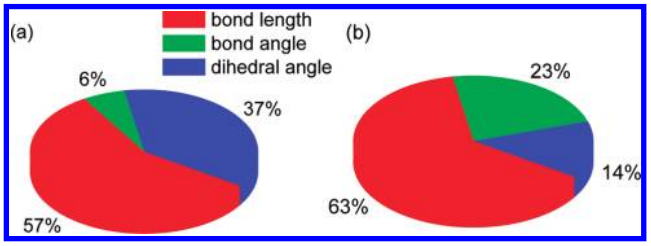

Figure 6. Contributions to the total reorganization energy from bond length, bond angle, and dihedral angle for (a) isolated **CPEI** molecule and (b) the molecule-in-cluster.

while for the cluster, those are mainly from the bond length (63%) associated with the C−C stretching vibration, the contribution that comes from the dihedral angle is only 14%. These results further confirm that the modes of rotation motions are crucial to determine the photophysical property.

V. CONCLUSIONS

In summary, we have theoretically investigated the aggregation effect on the photophysical properties of **CPEI** molecule employing the QM/MM approach and a distorted and displaced harmonic oscillator model. It is found that aggregation originated from intermolecular hydrogen-bonding interaction can largely suppress the nonradiative decay but does not much influence the radiative decay, thus increasing the fluorescence quantum yield by 1490 times from isolated molecule to aggregate state, in nice agreement with the experiment. It is found that in the solid state, the intermolecular hydrogen-bonding interaction makes the main conjugation backbone (C_1═C_2) close to planar and the intramolecular rotations are restricted by molecular packing. The N−H bond stretching mode in the gas phase is 3604 cm^{-1}, which is decreased to 3527 cm^{-1} in aggregate state, manifesting remarkable hydrogen-bonding interaction. Also, the fluorescence quantum yield is found to be insensitive to temperature in aggregate because of the hydrogen-bonding nature.

■ ASSOCIATED CONTENT

Supporting Information

Total energy and transition energy, normal-mode frequencies for S_0 and S_1, the selected Huang−Rhys factors, the component of reorganization energy in the selected internal coordinate representation, and the normal mode displacement vectors for the selected harmonic vibrational frequencies. This material is available free of charge via the Internet at http://pubs.acs.org.

■ AUTHOR INFORMATION

Corresponding Author

*E-mail: zgshuai@tsinghua.edu.cn.

Notes

The authors declare no competing financial interest.

■ ACKNOWLEDGMENTS

This work was supported by the China Postdoctoral Science Foundation, the National Natural Science Foundation of China (Grant Nos. 90921007, 20903102, and 21103097), and the Ministry of Science and Technology of China through 973 program (Grant Nos. 2009CB623600, 2011CB932304, and 2011CB808405). Discussions with Prof. Dongqi Wang on QM/MM are greatly acknowledged.

■ REFERENCES

(1) Luo, J.; Xie, Z.; Lam, J. W. Y.; Cheng, L.; Chen, H.; Qiu, C.; Kwok, H. S.; Zhan, X.; Liu, Y.; Zhu, D.; Tang, B. *Chem. Commun.* **2001**, 1740−1741.

(2) Tang, B.; Zhan, X.; Yu, G.; Lee, P.; Liu, Y.; Zhu, D. *J. Mater. Chem.* **2001**, *11*, 2974−2978.

(3) Yu, G.; Yin, S.; Liu, Y.; Chen, J.; Xu, X.; Sun, X.; Ma, D.; Zhan, X.; Peng, Q.; Shuai, Z.; Tang, B.; Zhu, D.; Fang, W.; Luo, Y. *J. Am. Chem. Soc.* **2005**, *127*, 6335−6346.

(4) Qin, A.; Lam, J. W. Y.; Mahtab, F.; Jim, C. K. W.; Tang, L.; Sun, J.; Sung, H. Y.; Williams, I. D.; Tang, B. *Appl. Phys. Lett.* **2009**, *94*, 253308.

(5) Li, Z.; Dong, Y.; Mi, B.; Tang, Y.; Häussler, M.; Tong, H.; Dong, Y.; Lam, J. W. Y.; Ren, Y.; Sun, H. H. Y.; Wong, K. S.; Gao, P.; Williams, I. D.; Kwok, H. S.; Tang, B. Z. *J. Phys. Chem. B* **2005**, *109*, 10061−10066.

(6) An, B.-K.; Kwon, S.-K.; Jung, S.-D.; Park, S. Y. *J. Am. Chem. Soc.* **2002**, *124*, 14410−14415.

(7) Liu, Y.; Tao, X.; Wang, F.; Shi, J.; Sun, J.; Yu, W.; Ren, Y.; Zou, D.; Jiang, M. *J. Phys. Chem. C* **2007**, *111*, 6544−6549.

(8) Sonoda, Y.; Tsuzuki, S.; Goto, M.; Tohnai, N.; Yoshida, M. *J. Phys. Chem. A* **2010**, *114*, 172−182.

(9) Hu, R.; Lager, E.; Aguilar-Aguilar, A.; Liu, J.; Lam, J. W. Y.; Sung, H. H. Y.; Williams, I. D.; Zhong, Y.; Wong, K. S.; Peña-Cabrera, E.; Tang, B. Z. *J. Phys. Chem. C* **2009**, *113*, 15845−15853.

(10) (a) Mitschke, U.; Bäuerle, P. J. *J. Mater. Chem.* **2000**, *10*, 1471−1507. (b) Chen, C.-T. *Chem. Mater.* **2004**, *16*, 4389−4400. (c) Veinot, J. G. C.; Marks, T. J. *Acc. Chem. Res.* **2005**, *38*, 632−643.

(11) (a) Sainova, D.; Miteva, T.; Nothofer, G.; Scherf, U.; Glowacki, I.; Ulanski, J.; Fujikawa, H.; Neher, D. *Appl. Phys. Lett.* **2000**, *76*, 1810−1812. (b) Hecht, S.; Frechet, J. M. J. *Angew. Chem., Int. Ed.* **2001**, *40*, 74−91.

(12) (a) Hide, F.; Diaz-Garcia, M. A.; Schwartz, B. J.; Heeger, A. J. *Acc. Chem. Res.* **1997**, *30*, 430−436. (b) Bunz, U. H. F. *Chem. Rev.*

2000, *100*, 1605−1644. (c) Hoeben, F. J. M.; Jonkheijm, P.; Meijer, E. W.; Schenning, A. P. H. J. *Chem. Rev.* **2005**, *105*, 1491−1546. (d) Thomas, S. W., III; Joly, G. D.; Swager, T. M. *Chem. Rev.* **2007**, *107*, 1339−1386. (e) Borisov, S. M.; Wolfbeis, O. S. *Chem. Rev.* **2008**, *108*, 423−461.

(13) Asefa, A.; Singh, A. K. *J. Lumin.* **2010**, *130*, 24−28.

(14) (a) Xiao, S.; Zou, Y.; Wu, J.; Zhou, Y.; Yi, T.; Li, F.; Huang, C. *J. Mater. Chem.* **2007**, *17*, 2483−2489. (b) Liu, Y.; Tao, X.; Wang, F.; Shi, J.; Sun, J.; Yu, W.; Ren, Y.; Zou, D.; Jing, M. *J. Phys. Chem. C* **2007**, *111*, 6544−6549. (c) He, J.; Xu, B.; Chen, F.; Xia, H.; Li, K.; Ye, L.; Tian, W. *J. Phys. Chem. C* **2009**, *113*, 9892−9899. (d) Zhou, T.; Li, F.; Fan, Y.; Song, W.; Mu, X.; Zhang, H.; Wang, Y. *Chem. Commun.* **2009**, 3199−3201. (e) Xu, B.; Fang, H.; Dong, Y.; Chen, F.; Chen, Q.; Sun, H.; Tian, W. *New J. Chem.* **2010**, *34*, 1838−1842. (f) Dai, Q.; Liu, W.; Zeng, L.; Lee, C. S.; Wu, J.; Wang, P. *CrysEngComm* **2011**, *13*, 4617−4624.

(15) Yin, S.; Peng, Q.; Shuai, Z.; Fang, W.; Wang, Y.; Luo, Y. *Phys. Rev. B* **2006**, *73*, 205409.

(16) Peng, Q.; Yi, Y.; Shuai, Z.; Shao, J. *J. Am. Chem. Soc.* **2007**, *129*, 9333−9339.

(17) Deng, C.; Niu, Y.; Peng, Q.; Qin, A.; Shuai, Z.; Tang, B. Z. *J. Chem. Phys.* **2011**, *135*, 014304.

(18) (a) Bernardi, F.; De, S.; Olivucci, M.; Robb, M. A. *J. Am. Chem. Soc.* **1990**, *112*, 1737−1744. (b) Reguero, M.; Olivucci, M.; Bernardi, F.; Robb, M. A. *J. Am. Chem. Soc.* **1994**, *116*, 2103−2114. (c) Bearpark, M. J.; Bernardi, F.; Clifford, S.; Olivucci, M.; Robb, M. A.; Smith, B. R.; Vreven, T. *J. Am. Chem. Soc.* **1996**, *118*, 169−175. (d) Vallet, V.; Lan, Z.; Mahapatra, S.; Sobolewski, A. L.; Domcke, W. *J. Chem. Phys.* **2005**, *123*, 144307. (e) Levine, B. G.; Martinez, T. J. *Annu. Rev. Phys. Chem.* **2007**, *58*, 613−634. (f) Duncan, W. R.; Prezhdo, O. V. *Annu. Rev. Phys. Chem.* **2007**, *58*, 143−184. (g) Lan, Z.; Fabiano, E.; Thiel, W. *J. Phys. Chem. B* **2009**, *113*, 3548−3555.

(19) (a) Meyer, H.-D.; Miller, W. H. *J. Chem. Phys.* **1980**, *72*, 2272−2281. (b) Salek, P.; Vahtras, O.; Helgaker, T.; Ågren, H. *J. Chem. Phys.* **2002**, *117*, 9630−9645. (c) Subotnik, J. E. *J. Chem. Phys.* **2010**, *132*, 134112.

(20) (a) Tully, J. C. *J. Chem. Phys.* **1990**, *93*, 1061−1071. (b) Hammes-Schiffer, S.; Tully, J. C. *J. Chem. Phys.* **1994**, *101*, 4657−4667. (c) Prezhdo, O. V. *J. Chem. Phys.* **1999**, *111*, 8366−8377. (d) Schmidt, J. R.; Parandekar, P. V.; Tully, J. C. *J. Chem. Phys.* **2008**, *129*, 044104.

(21) Meyer, H. D.; Manthe, U.; Cederbaum, L. S. *Chem. Phys. Lett.* **1990**, *165*, 73−78.

(22) (a) Manthe, U.; Meyer, H. D.; Cederbaum, L. S. *J. Chem. Phys.* **1992**, *97*, 3199−3213. (b) Worth, G.; Meyer, H.-D.; Cederbaum, L. S. *J. Chem. Phys.* **1998**, *109*, 3518−3529. (c) Raab, A.; Worth, G. A.; Meyer, H.-D.; Cederbaum, L. S. *J. Chem. Phys.* **1999**, *110*, 936−946. (d) Beck, M. H.; Jäckle, A.; Worth, G. A.; Meyer, H.-D. *Phys. Rep.* **2000**, *324*, 1−105. (e) Worth, G. A.; Meyer, H.-D.; Köppel, H.; Cederbaum, L. S.; Burghardt, I. *Int. Rev. Phys. Chem.* **2008**, *27*, 569−606.

(23) Turro, N. J.; Ramamurthy, V.; Scaiano, J. C. *Modern Molecular Photochemistry of Organic Molecules*; University Science Books: Sausalito, CA, 2009; Chapter 4.

(24) Jiang, Y. Q.; Peng, Q.; Gao, X.; Shuai, Z. G.; Niu, Y. L.; Lin, S. H. *J. Mater. Chem.* **2012**, *22*, 4491.

(25) (a) Tang, J.; Lee, M. T.; Lin, S. H. *J. Chem. Phys.* **2003**, *119*, 7188. (b) Ianconescu, R.; Pollak, E. *J. Phys. Chem. A* **2004**, *108*, 7778. (c) Li, M. C.; Hayashi, M.; Lin, S. H. *J. Phys. Chem. A* **2011**, *115*, 14531.

(26) Niu, Y.; Peng, Q.; Deng, C.; Gao, X.; Shuai, Z. *J. Phys. Chem. A* **2010**, *114*, 7817−7831.

(27) Huang., K.; Rhys, A. *Proc. R. Soc. London, Ser. A* **1951**, *208*, 352.

(28) (a) Lin, S. H. *J. Chem. Phys.* **1966**, *44*, 3759. (b) Hayashi, M.; Mebel, A. M.; Liang, K. K.; Lin, S. H. *J. Chem. Phys.* **1998**, *108*, 2044−2055. (c) Mebel, A. M.; Hayashi, M.; Liang, K. K.; Lin, S. H. *J. Phys. Chem. A* **1999**, *103*, 10674−10690.

(29) (a) Peng, Q.; Yi, Y.; Shuai, Z.; Shao, J. *J. Chem. Phys.* **2007**, *126*, 114302. (b) Müller, C. W.; Newby, J. J.; Liu, C.-P.; Rodrigo, C. P.; Zwier, T. S. *Phys. Chem. Chem. Phys.* **2010**, *12*, 2331−2343.

(30) Niu, Y.; Peng, Q.; Shuai, Z. *Sci. China, Ser. B: Chem.* **2008**, *51*, 1153−1158.

(31) Reimers, J. R. *J. Chem. Phys.* **2001**, *115*, 9103−9019.

(32) (a) Ahlrichs, R.; Bar, M.; Haser, M.; Horn, H.; Kolmel, C. *Chem. Phys. Lett.* **1989**, *162*, 165−169. (b) Deglmann, P.; Furche, F. *J. Chem. Phys.* **2002**, *117*, 9535−9538. (c) Deglmann, P.; Furche, F.; Ahlrichs, R. *Chem. Phys. Lett.* **2002**, *362*, 511−518. (d) Furche, F.; Ahlrichs, R. *J. Chem. Phys.* **2002**, *117*, 7433−7447.

(33) (a) Dreuw, A.; Head-Gordon, M. *Chem. Rev.* **2005**, *105*, 4009−4037. (b) Serrano-Andres, L.; Merchan, M. *J. Mol. Struct. (THEOCHEM)* **2005**, *729*, 99−108.

(34) (a) French, S. A.; Sokol, A. A.; Bromley, S. T.; Catlow, C. R. A.; Rogers, S. C.; King, F.; Sherwood, P. *Angew. Chem., Int. Ed.* **2001**, *40*, 4437−4440. (b) Acevedo, O.; Jorgensen, W. L. *J. Am. Chem. Soc.* **2006**, *128*, 6141−6146. (c) To, J.; Sherwood, P.; Sokol, A. A.; Bush, I. J.; Catlow, C. R. A.; van Dam, H. J. J.; French, S. A.; Guest, M. F. *J. Mater. Chem.* **2006**, *16*, 1919−1926. (d) Tsushima, S.; Wahlgren, U.; Grenthe, I. *J. Phys. Chem. A* **2006**, *110*, 9175−9182. (e) Senn, H. M.; Thiel, W. *Curr. Opin. Chem. Biol.* **2007**, *11*, 182−187. (f) Lin, H.; Truhlar, D. G. *Theor. Chem. Acc.* **2007**, *117*, 185−199. (g) Torras, J.; Bromley, S.; Bertran, O.; Illas, F. *Chem. Phys. Lett.* **2008**, *457*, 154−158. (h) Senn, H. M.; Thiel, W. *Angew. Chem., Int. Ed.* **2009**, *48*, 1198−1229. (i) Parac, M.; Doerr, M.; Marian, C. M.; Thiel, W. *J. Comput. Chem.* **2010**, *31*, 90−106.

(35) Sherwood, P.; et al. *J. Mol. Struct. (THEOCHEM)* **2003**, *632*, 1−28.

(36) Billeter, S. R.; Turner, A. J.; Thiel, W. *Phys. Chem. Chem. Phys.* **2000**, *2*, 2177−2186.

(37) Smith, W.; Forester, T. R. *J. Mol. Graphics* **1996**, *14*, 136−141.

(38) Wang, J.; Wolf, R. M.; Caldwell, J. W.; Kollamn, P. A.; Case, D. A. *J. Comput. Chem.* **2004**, *25*, 1157−1174.

(39) Bakowies, D.; Thiel, W. *J. Phys. Chem.* **1996**, *100*, 10580−10594.

(40) Frisch, M. J.; et al. *Gaussian 09*; Gaussian, Inc.: Wallingford, CT, 2009.

(41) Werner, H.-J.; Knowles, P. J.; Lindh, R.; Manby, F. R.; Schütz, M. *MOLPRO, version 2010.1, a package of ab initio programs*, 2010; http://www.molpro.net.

(42) (a) Spano, F. *Acc. Chem. Res.* **2010**, *43*, 429−439. (b) Gao, F.; Zhao, Y.; Liang, W. Z. *J. Phys. Chem. B* **2011**, *115*, 2699.